3-D ELECTROSTATIC AND ELECTROMAGNETIC RAY TRACING IN THE MAGNETOSPHERE

Kimiya YAMAASHI[1]*, Kozo HASHIMOTO[2] and Iwane KIMURA[1,3]

[1] *Department of Electrical Engineering II, Kyoto University,*
Yoshida Honmachi, Sakyo-ku, Kyoto 606
[2] *Department of Electrical Engineering, Tokyo Denki University,*
2, Kanda Nishikicho 2-chome, Chiyoda-ku, Tokyo 101
[3] *Institute of Space and Astronautical Science,*
6-1, Komaba 4-chome, Meguro-ku, Tokyo 153

Abstract: A three-dimensional (3-D) ray tracing computer program has been developed, which is applicable to both electrostatic and electromagnetic mode waves, using the hot plasma dispersion relation. This program is able to deal with, for example, a mode conversion process of a wave through propagation in an inhomogeneous medium, such as a smooth conversion from the electrostatic electron cyclotron harmonic mode to the electromagnetic (R-X-Z) mode in a hot plasma. For a sufficiently large wave number region, the electrostatic approximation is also used to trace ray paths. This approximation is, for example, useful to investigate the necessary initial conditions for the mode conversion from the electrostatic mode to the electromagnetic mode. This approximation clarifies that the electron cyclotron harmonic mode waves can propagate over a long distance if the starting point is in a very vicinity of the geomagnetic equator and the wave normal direction is almost perpendicular to the geomagnetic field line. For the mode conversion, the inital wave normal vector must be almost in the meridian plane in addition to the above conditions.

1. Introduction

Ray tracing technique has been widely used in large extents of electromagnetic modes, such as HF waves in the ionosphere and whistler mode waves (*e.g.* KIMURA, 1985) and auroral kilometric radiation (*e.g.* HASHIMOTO, 1985) in the ionosphere and magnetosphere. However most of ray tracing has been performed in a cold plasma. One of the electrostatic cyclotron harmonic modes above the electron cyclotron frequency, is connected continuously to an electromagnetic mode with a small wave number through the upper hybrid resonance. The rest of the modes are purely electrostatic.

Ray tracing of electrostatic cyclotron harmonic waves was done graphically by LEMBEGE and JONES (1982) using Poeverlein's construction method. In order to consider Z-mode waves converted from electrostatic waves, the results of the electrostatic ray tracing were used as the initial conditions for a cold plasma ray tracing of the Z mode. In this work, it was assumed that both the cold plasma (electromagnetic) mode and electrostatic mode can exist at the junction point. BARBOSA and KURTH (1980) calculated ray paths of electrostatic cyclotron harmonic waves, using the

---

* Now at Hitachi Research Laboratory, Hitachi Co. Ltd., Hitachi, Ibaraki 319–12.

electrostatic dispersion relation, for $f_c < f \ll f_p$ in the Jovian magnetosphere under a constant electron density model.

Ray tracing in a hot plasma without any electrostatic approximation is necessary to confirm a smooth conversion between the cyclotron mode and the Z mode. OHNUMA et al. (1982) developed a ray tracing program in a slab hot plasma with a Gaussian electron density distribution. They have not assumed any electrostatic approximation. They, however, made ray tracing only in an electrostatic range.

In order to study propagation of electrostatic waves and a mode conversion process from the electrostatic electron cyclotron mode to the electromagnetic mode through an inhomogeneous medium, we have developed a three dimensional (3-D) ray tracing program which is able to continuously treat both the electrostatic electron cyclotron (harmonic) mode and electromagnetic (R-X-Z) mode under a realistic magnetospheric model.

In the present study, a 3-D ray tracing program has been developed first under the electrostatic approximation, and then for the dispersion relation in a hot plasma without the approximation in a Maxwellian electron distribution function.

2. Ray Tracing Technique in Hot Plasma

2.1. Basic equations for ray tracing

Basic equations of ray tracing governing ray path vector r and wave normal vector k are (WEINBERG, 1962)

$$\frac{dr}{d\tau} = \frac{\partial D}{\partial k}, \tag{1}$$

$$\frac{dk}{d\tau} = -\frac{\partial D}{\partial r}, \tag{2}$$

where

$$D(r, k\, \omega) = \text{constant}, \tag{3}$$

is the dispersion relation. ω is the wave frequency and τ is a quantity proportional to the phase propagation time. A ray path is obtained by a simultaneous integration of the right-hand side of the above eqs. (1) and (2) by τ using the Adams method. In a hot plasma, the dispersion relation generally provide a complex k or n ($=ck/\omega$). However, if the imaginary part of k or the imaginary part (χ) of the refractive index ($n = \mu - i\chi$) is relatively large, the ray path thus obtained becomes meaningless. Therefore we have to check at every step of integration if the quantity χ is much smaller than the real part μ of n. The real propagation time t can be calculated by integrating the following differential equation

$$\frac{dt}{d\tau} = -\frac{\partial D}{\partial \omega}. \tag{4}$$

For three dimensional ray tracing two coordinate systems are used; one is the X, Y, Z orthogonal coordinate system with the origin located at earth's center, to re-

present ray path in which Z axis is directed to the geomagnetic north and X and Y axes are directed to the geomagnetic equator at a longitude of $0°$ and $90°$, respectively. An instantaneous ray path vector r from the origin in this coordinate system makes an angle θ with Z axis and its projection on the X-Y plane shows an angle ϕ with X axis.

For calculating the right hand side of eqs. (1) and (2), another local orthogonal coordinate system (see Fig. 1) is convenient, in which the z axis is directed to the geomagnetic field (B), the x axis is orthogonal to the z axis in the meridional plane and the y axis completes a right-hand coordinate system with the above x and z axes. In this local system k vector makes an angle ϕ with z axis (B) and its projection onto the x-y plane shows an angle η with x axis. ϕ and η are the wave normal angle and the azimuth angle of the ray path vector, respectively. The right-hand sides of eqs. (1) and (2) are calculated in this local system because the dispersion relation is dependent on the angle ϕ. Then the left hand side of eqs. (1) and (2) which are defined in the X, Y, Z coordinate system, can be obtained by an appropriate coordinate transformation from the quantities defined in the local system, as follows.

$$
\begin{pmatrix} \dfrac{dX}{d\tau} \\[2mm] \dfrac{dY}{d\tau} \\[2mm] \dfrac{dZ}{d\tau} \end{pmatrix} = \begin{pmatrix} \dfrac{\partial D}{\partial k_x} \\[2mm] \dfrac{\partial D}{\partial k_y} \\[2mm] \dfrac{\partial D}{\partial k_z} \end{pmatrix} = \begin{pmatrix} \dfrac{\partial k}{\partial k_x} & \dfrac{\partial \phi}{\partial k_x} \\[2mm] \dfrac{\partial k}{\partial k_y} & \dfrac{\partial \phi}{\partial k_y} \\[2mm] \dfrac{\partial k}{\partial k_z} & \dfrac{\partial \phi}{\partial k_z} \end{pmatrix} \begin{pmatrix} \dfrac{\partial D}{\partial k} \\[6mm] \dfrac{\partial D}{\partial \phi} \end{pmatrix} \tag{5}
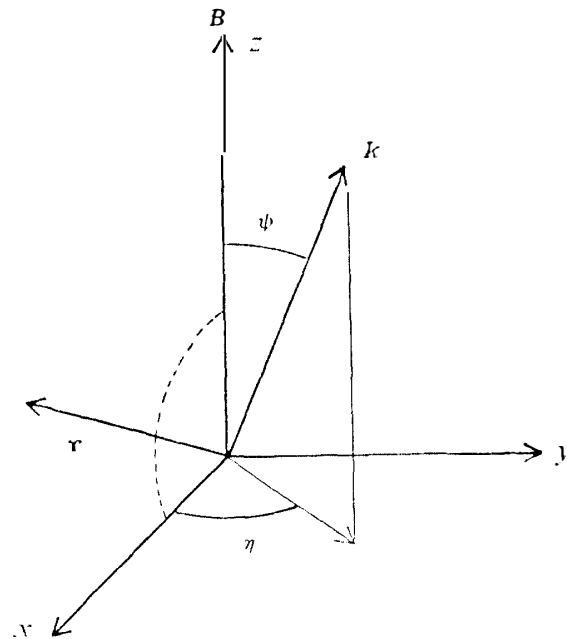$$

Fig. 1. Wave number vector and coordinate system referred to the geomagnetic field.

$$\begin{pmatrix} \dfrac{\mathrm{d}k_X}{\mathrm{d}\tau} \\[2mm] \dfrac{\mathrm{d}k_Y}{\mathrm{d}\tau} \\[2mm] \dfrac{\mathrm{d}k_Z}{\mathrm{d}\tau} \end{pmatrix} = - \begin{pmatrix} \dfrac{\partial D}{\partial X} \\[2mm] \dfrac{\partial D}{\partial Y} \\[2mm] \dfrac{\partial D}{\partial Z} \end{pmatrix} = - \begin{pmatrix} \sin\theta\cos\phi & \cos\theta\cos\phi & -\sin\phi \\[1mm] \sin\theta\sin\phi & \cos\theta\sin\phi & \cos\phi \\[1mm] \cos\theta & -\sin\theta & 0 \end{pmatrix} \begin{pmatrix} \dfrac{\partial D}{\partial r} \\[2mm] \dfrac{1}{r}\dfrac{\partial D}{\partial\theta} \\[2mm] \dfrac{1}{r\sin\theta}\dfrac{\partial D}{\partial\phi} \end{pmatrix} . \qquad (6)$$

In dealing with the waves in a hot plasma, we first adopt the electrostatic approximation for the dispersion relation and as the second step a full hot plasma dispersion relation is used.

2.2. Electrostatic approximation

In the following we neglect the effect of ions and assume the isotropic Maxwellian distribution with no drift velocity, then the dispersion relation in the electrostatic approximation is given by (e.g. MIYAMOTO, 1976, chapt. 11)

$$D = (k\rho)^2 + \left(\frac{\Pi}{\Omega}\right)^2 \left\{ 1 + \sum_{n=-\infty}^{\infty} \left(1 - \frac{n\Omega}{\omega+n\Omega}\right) I_n(b) e^{-b} \zeta_n Z(\zeta_n) \right\} = 0 , \qquad (7)$$

where

$$b = (k\rho\sin\phi)^2 , \quad \text{and} \quad \zeta_n = \frac{\omega+n\Omega}{\sqrt{2}\,k\rho\Omega\cos\phi} . \qquad (8)$$

In the above equation, Π and Ω are the electron plasma and cyclotron frequencies, ρ is the Larmor radius defined by v_T/Ω, $v_T = \sqrt{(T/m)}$ and $Z(\zeta_n)$ is the so-called plasma dispersion function.

When $|\phi| \le 90°$ and $I_m(\zeta) > 0$, the dispersion function $Z(\zeta_n)$ is approximated by

$$Z(\zeta) = Z_p(\zeta) \equiv \frac{1}{\sqrt{\pi}} \int_{-\infty}^{\infty} \frac{\exp(-\beta^2)}{\beta-\zeta}\,\mathrm{d}\beta , \qquad (9)$$

which can be analytically continued to the region for $I_m(\zeta) \le 0$. And we can use the following asymptotic expansion,

$$Z_p(\zeta) = i\sqrt{\pi}\,\sigma\,\exp(-\zeta^2) - \frac{1}{\zeta}\left(1 + \frac{1}{2\zeta^2} + \frac{3}{4\zeta^4} + \cdots\right) , \qquad (10)$$

$$\sigma = \begin{cases} 0 & I_m(\zeta) > 0 \\ 1 & I_m(\zeta) = 0 \\ 2 & I_m(\zeta) < 0 . \end{cases} \qquad (11)$$

For $|\phi| > 90°$, the dispersion function $Z(\zeta)$ can be expressed by

$$Z(\zeta) = Z_p(\zeta) - 2i\sqrt{\pi}\,\exp(-\zeta^2) . \qquad (12)$$

The electrostatic waves can exist only for $\phi \simeq 90°$, where $\cos\phi \to 0$ and ζ_n increases to infinity. Therefore, for eq. (7), the above expansion will be better expressed by

$$\zeta_n Z(\zeta_n) \simeq -\left(1 + \frac{1}{2\zeta_n^2} + \frac{3}{4\zeta_n^4} + \cdots\right) . \qquad (13)$$

This approximated dispersion relation is much simpler than the following hot plasma dispersion relation and can save computer time in ray tracing.

2.3. Ray tracing using the full dispersion in hot plasma

The dispersion relation in a hot plasma without any electrostatic approximation is given by (MIYAMOTO, 1976, chapt. 13)

$$D=\begin{vmatrix} H_{xx}-k^2+(\omega/c)^2 & H_{xy} & H_{xz} \\ -H_{xy} & H_{yy}-k^2\cos^2\psi+(\omega/c)^2 & H_{yz}+k^2\sin\psi\cos\psi \\ -H_{xz} & H_{yz}+k^2\sin\psi\cos\psi & H_{zz}-k^2\sin^2\psi+(\omega/c)^2 \end{vmatrix}=0, \quad (14)$$

$$H=\left(\frac{\Pi}{c}\right)^2\sum_n\{\zeta_0 Z(\zeta_n)\}\,e^{-b}X_n+2\zeta_0^2\,L\,, \tag{15}$$

where

$$\alpha=k\rho\sin\psi\,,\quad b=\alpha^2\,,\quad \rho=v_T/\Omega\,, \tag{16}$$

and

$$X_n=\begin{pmatrix} \left(\frac{n^2}{b}+2b\right)I_n(b)-2bI_n'(b) & in\{I_n'(b)-I_n(b)\} & -i\sqrt{2}\,\zeta_n\alpha\{I_n'(b)-I_n(b)\} \\ -in\{I_n'(b)-I_n(b)\} & \frac{n^2}{b}I_n(b) & -\sqrt{2}\,\zeta_n\frac{n}{\alpha}I_n(b) \\ i\sqrt{2}\,\zeta_n\alpha\{I_n'(b)-I_n(b)\} & \sqrt{2}\,\zeta_n\frac{n}{\alpha}I_n(b) & 2\zeta_n^2 I_n(b) \end{pmatrix}, \tag{17}$$

$I_n(b)$ is the modified Bessel function of order n, and L is a tensor, in which all elements are zero except $L_{zz}=1$.

For $|\psi|\sim90°$, the asymptotic expansion of the plasma dispersion function (10) leads to

$$H=\left(\frac{\Pi}{c}\right)^2\sum_n\left\{\frac{\omega}{\omega_n}(Y_{1n}-Y_{2n})\right\}, \tag{18}$$

$$Y_{1n}=\frac{\varepsilon_n}{\zeta_n^2}\begin{pmatrix} Y_{xx} & Y_{xy} & \zeta_n Y_{xz} \\ Y_{yx} & Y_{yy} & \zeta_n Y_{yz} \\ \zeta_n Y_{zx} & \zeta_n Y_{zy} & \zeta_n^2 Y_{zz} \end{pmatrix}, \quad Y_{2n}=\begin{pmatrix} Y_{xx} & Y_{xy} & 0 \\ Y_{yx} & Y_{yy} & 0 \\ 0 & 0 & 0 \end{pmatrix}, \tag{19}$$

$$\varepsilon_n=\zeta_n^2\{1+\zeta_n Z(\zeta_n)\}\simeq-\frac{1}{2}-\frac{1}{4\zeta_n^2}-\cdots\,,\quad \omega_n=\omega+n\Omega\,, \tag{20}$$

$$Y=\begin{pmatrix} \left(\frac{n^2}{b}+2b\right)I_n(b)-2bI_n'(b) & in\{I_n'(b)-I_n(b)\} & -i\sqrt{2}\,\alpha\{I_n'(b)-I_n(b)\} \\ -in\{I_n'(b)-I_n(b)\} & \frac{n^2}{b}I_n(b) & -\sqrt{2}\,\frac{n}{\alpha}I_n(b) \\ i\sqrt{2}\,\alpha\{I_n'(b)-I_n(b)\} & -\sqrt{2}\,\frac{n}{\alpha}I_n(b) & \sqrt{2}\,I_n(b) \end{pmatrix}. \tag{21}$$

To evaluate the right hand side of eqs. (1) and (2), derivatives of D with respect to r, and k are required.   The derivatives with respect to (r,θ,ϕ) coordinates can be calculated when a plasma density distribution and a geomagnetic field model are given.

The derivatives with respect to k can be calculated analytically from the dispersion relation.

This ray tracing is commonly used in both electrostatic and electromagnetic regions, so that we can use it to study a situation, in which an electrostatic wave generated somewhere propagates in an inhomogeneous medium to be converted to an electromagnetic wave.

3.   Results of Ray Tracing

3.1.   Electron density profile and geomagnetic field model

LEMBEGE and JONES (1982) made ray tracing for electrostatic cyclotron harmonic
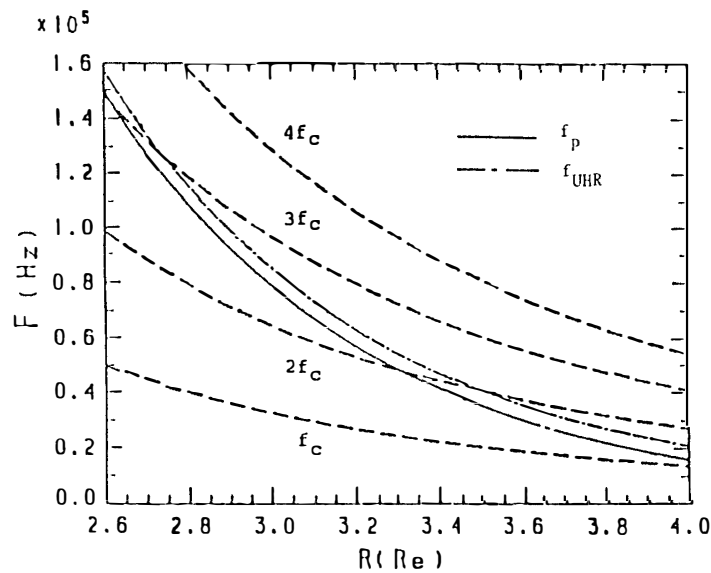
Fig. 2.   Electron density profile (the solid line). f_c shows the cyclotron frequency, and the dot-dash line indicates the upper hybrid frequency.
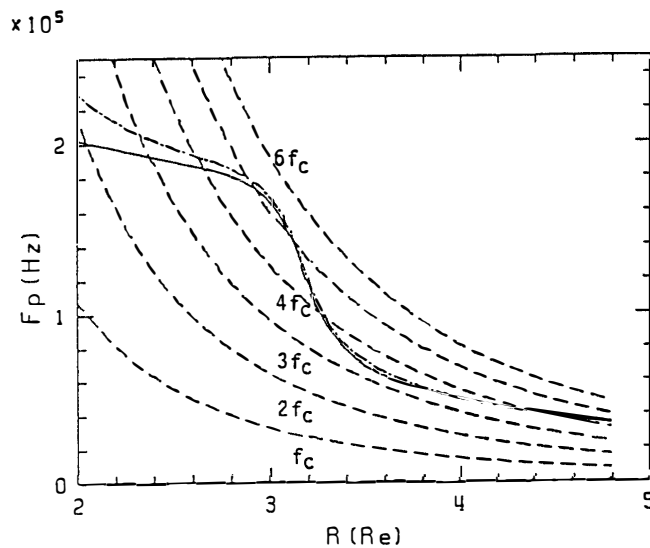

Fig. 3.   Electron density (solid line) profile and f_{UHR} (dot-dash line) with the plasmapause. The plasmapause is at $L=3.14$.

waves using Poeverlein's construction method. They used a density profile deduced from continuum radiation spectra (JONES, 1981). We use the following equation based on their density profile.

$$N_e = 1.14 \times 10^6 \exp\left(-3.2\, R/R_e\right) \quad [\mathrm{cm}^{-3}], \tag{22}$$

where R is the radial distance and R_e is the earth radius. In Fig. 2, the solid line shows the plasma frequency f_p deduced from this N_e as a function of equatorial radial distance. In the figure the electron cyclotron frequency f_c and its harmonics are drawn by borken lines and the upper hybrid frequency f_{UHR} is also shown by a dot-dash line.

In addition to the electron density model represented by eq. (22), an electron density model with the plasmapause at $L=3.14$ is used, based on AIKYO and ONDOH (1971). In Fig. 3, the plasma frequency deduced from this electron density profile, and other parameters are drawn in the same manner as in Fig. 2. The dipole magnetic field model is adopted for our ray tracing.

3.2.   Ray paths under electrostatic approximation

3.2.1.   2-D ray tracing in no plasmapause model

The electrostatic approximation much more simplifies the ray tracing; we can obtain correct ray paths for electrostatic waves by this approximation insofar as $|k|$ is large enough. The electron temperature is assumed to be 12000 K. The range where this approximation is valid is $k\rho > 1$. For example, we consider the ω-k diagrams without the approximation of two cases as shown in Figs. 4a and 4b, where the plasma frequency f_p and upper hybrid frequency f_{UHR} are between once and twice the electron cyclotron frequency f_c in Fig. 4a and are between twice and three times the cyclotron frequency in Fig. 4b.
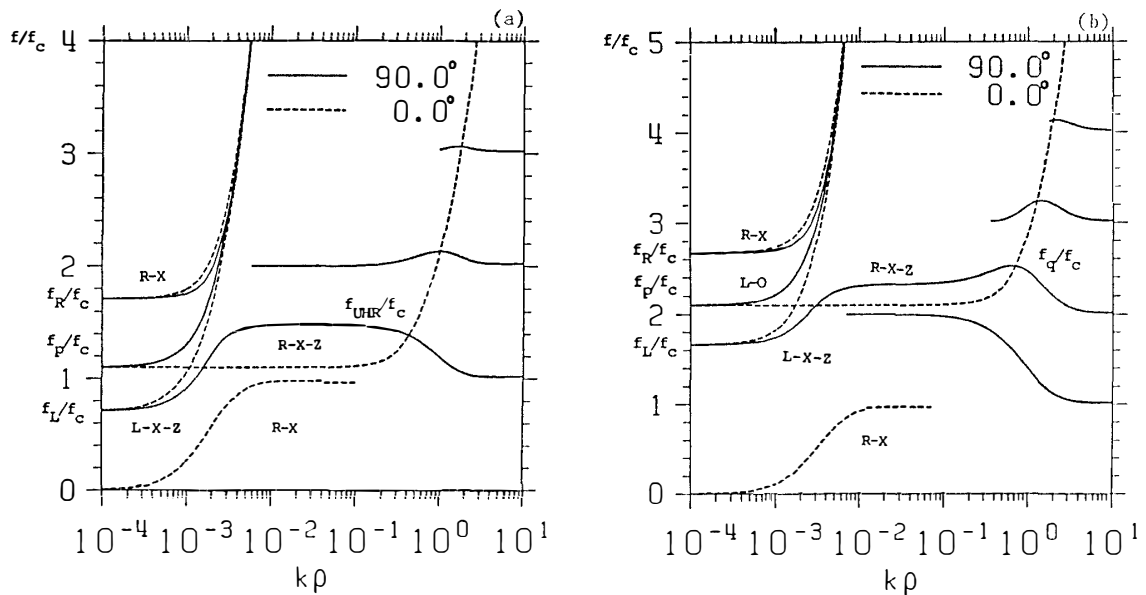

Fig. 4.   Dispersion curves in a hot plasma.   (a) $f_c < f_p$, $f_{UHR} < 2f_c$.   (b) $2f_c < f_p$, $f_{UHR} < 3f_c$. f_R and f_L are the cutoff frequencies of the right-handed and left-handed polarized modes respectively, and f_q is the resonance frequency where the group velocity becomes zero.

We are interested in an electrostatic branch connected to the Z mode for $\phi \sim 90°$ at f_{UHR} in the above two cases. The approximations are valid when $k\rho$ is larger than that for $f \simeq f_{\mathrm{UHR}}$. Then $k\rho$ must be larger than 0.1. In case Fig. 4b, the ray velocity, the component of the group velocity in the wave normal direction, $\partial\omega/\partial k$ becomes zero at f_{q} resonance frequency as well as at f_{UHR}.
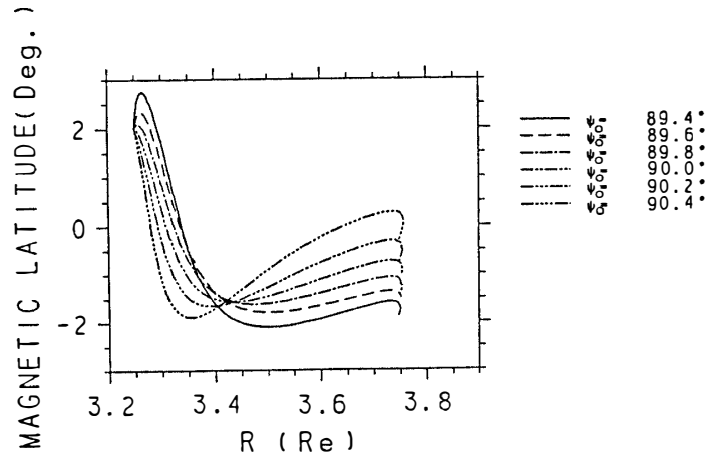

Fig. 5. *Dependence of the ray paths on the initial wave normal angle. The wave frequency is 28.015 kHz and the starting point locations are R=3.25 R_e and a geomagnetic latitude of 2°. The initial wave normal angle ϕ selected is in the range 89.4–90.4°.*

Figure 5 illustrates six ray paths for a plasma temperature of 12000 K in the electron density profile shown in Fig. 2, where the abscissa is the radial distance normalized by R_e and the ordinate is the geomagnetic latitude. The starting points are located at $R=3.25\,R_\mathrm{e}$ and at a geomagnetic latitude of 2°. The wave frequency selected is 28.015 kHz and the azimuth angle (η_0) is 180° from the radial direction. Various initial wave normal angles with respect to the geomagnetic field direction ϕ_0 are selected in a range from 89.4° to 90.4°. At the starting point, $f_\mathrm{p} \sim 2.1 f_\mathrm{e}$, so that $f \sim 1.1 f_\mathrm{e}$. Shown in Fig. 5 are the ray paths which are traced either until $k\rho$ becomes very small, where the approximation becomes invalid, or while the imaginary part of the refractive index is small, *i.e.* $\chi/\mu < 10^{-4}$. These paths move toward higher latitude first, and soon they changes the direction toward lower latitude and are trapped near the equator.

In Fig. 6, ray paths starting from $R=3.25\,R_\mathrm{e}$ at various latitudes ranged from $-5°$ to 5° are shown. In each panel from Fig. 6a to 6e, the frequency is different and the relative frequency to the electron cyclotron frequency at the initial point is ranged from 1.1 to 1.5. Other conditions are unchanged from those shown in Fig. 5. From these figures, it is clear that the ray paths starting in the vicinity of the geomagnetic equatorial plane (with initial latitude within $\pm 2° \sim 3°$), especially for low frequencies (case a and b), are focused around the equator and can propagate over a long distance up to $R \sim 3.75\,R_\mathrm{e}$, whereas those starting at higher latitudes stop propagation within a short distance due to wave damping, because the wave normal direction quickly depart from 90° in propagation for the paths with the initial latitudes larger than $2° \sim 3°$.

Dependence of initial latitude shown in Fig. 6a is easily understood from Fig. 7, where the refractive index surface and evolution of instantaneous wave normal direction
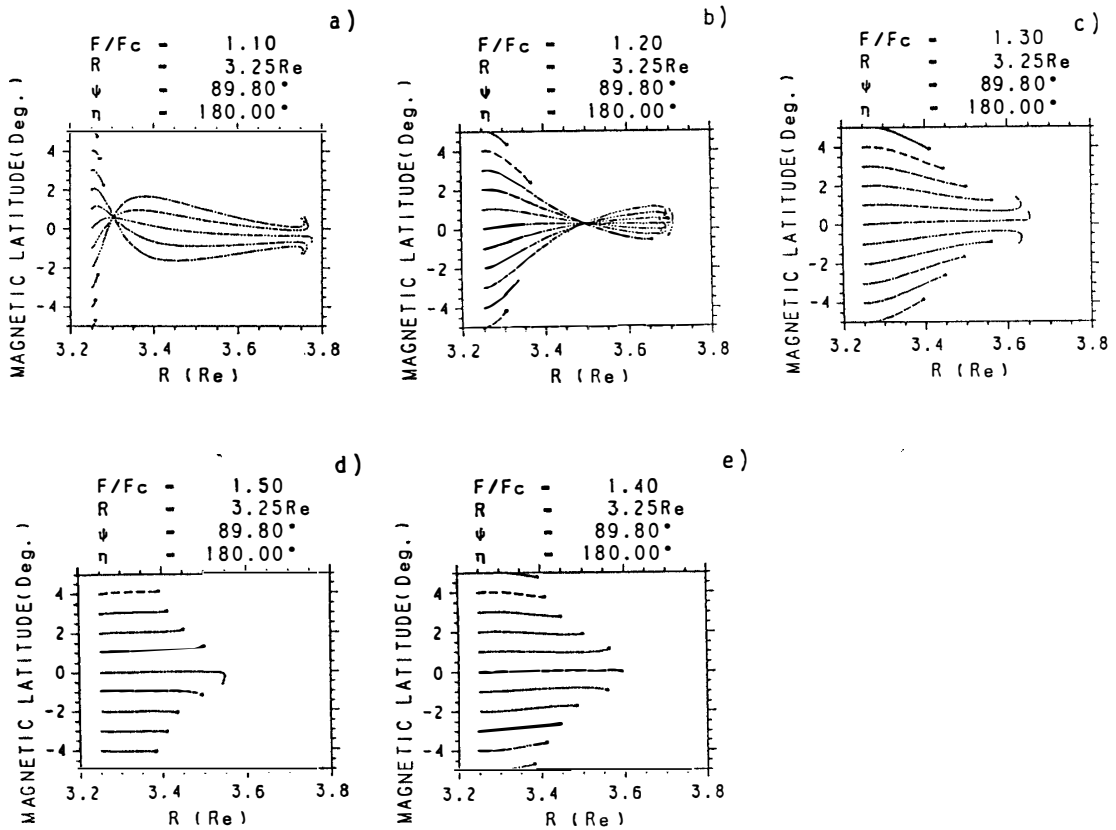
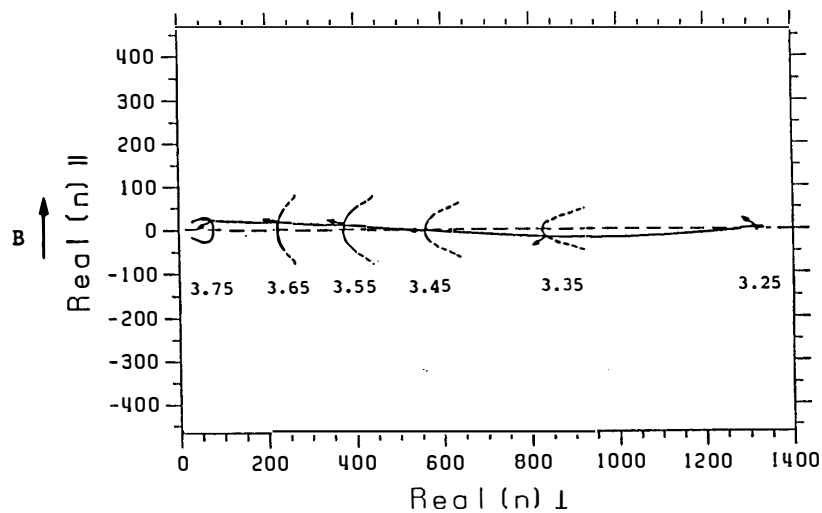*Fig. 6.   Dependence of the ray paths on the frequency and the initial latitude.*

Fig. 7.   Refractive index surface and instantaneous ray direction for the path shown in Fig. 6a. The initial wave normal angle is 89.8°.

(η=180°) along the path from R=3.25 to 3.75 R_e as shown by the path starting at a latitude of 2° in Fig. 6a are illustrated on the real $n_\perp$-real $n_{||}$ plane.

Snell's law requests that the component of k perpendicular to ∇B be conserved during propagation if ∇N_e is small.   The angle ψ can be 90° in the dipole model be-

cause ∇B direction is not necessarily perpendicular to B. ϕ starts from 89.8°, increases up to 90° and then decreases. The direction of ∇B depends on latitude and is not constant.

3.2.2. 3-D ray tracing in no plasmapause model

Next we will show an example of 3-D ray paths in Fig. 8, where the initial azimuth angle (η_0) is varied from 180° to 160°, with the initial $\phi_0 = 89.8°$, and other initial conditions are the same as those used in Fig. 5. The solid lines in the figures correspond to $\eta = 180°$, whereas the dashed lines and the dot-dash lines correspond to 170° and 160°, respectively. It is evident that those for off-meridional initial directions reflect by refraction at certain radial distances back to the original radial distance with different longitude or meridional distance Y, as shown in Fig. 8a. Figure 8b illustrates the paths in the X-Z plane which corresponds to radius vs. latitude plane in the previous figures. In Fig. 8c the real part of ($k\rho$) is shown as a function of propagation
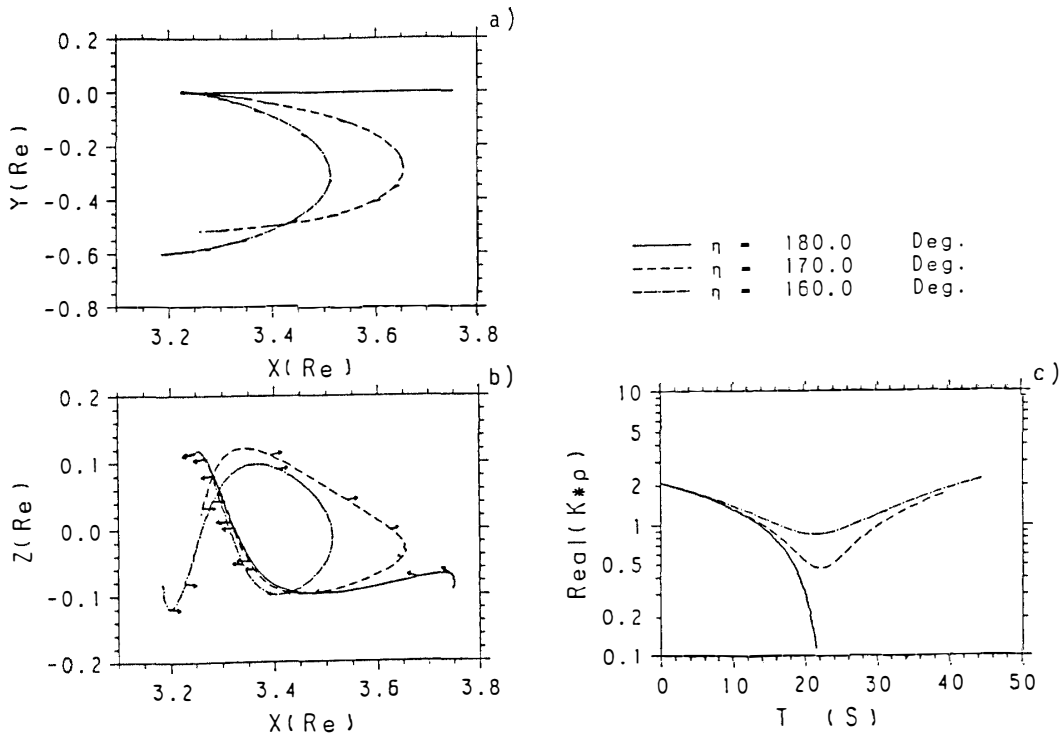

Fig. 8. Dependence of 3-D ray paths on the azimuth angle of the initial wave normal direction. The wave frequency and the starting point location are the same as those for Fig. 5 and the initial wave normal angle is 89.8°.

time. These figures suggest that for the off-meridional initial directions the value of $k\rho$ exceeds certain value and the path cannot reach electromagnetic region (with small $k\rho$). Therefore we can conclude that a necessary condition for energy conversion from a electrostatic mode wave to an electromagnetic mode wave through a continuous branch (the upper hybrid resonance) is that the initial wave normal direction is almost in the meridian plane with initial latitude close to the geomagnetic equatorial plane.

The existence of minimum $k\rho$ for the off-meridional propagation can also be ex-

plained by Snell's law.   In the equator, both the direction of ∇B and that of ∇N_e are same.   The component perpendicular to this direction of k must be conserved.   This is the off-meridional component of k and decides the minimum value of k or $k\rho$.

3.2.3.   2-D ray tracing in plasmapause model

As the next step, ray tracing in the electron density profile with a plasmapause at $L=3.14$ is made.   The used electron density profile is shown in Fig. 3.   In Fig. 9c, a ray path for a frequency $f=5.15 f_c$ or equal to the local f_{UHR} starting from $R=3.10\,R_e$ and a geomagnetic latitude of $0°$ is shown.   Variations of parameters along the ray path are also shown in the other panels of Fig. 9.   The initial wave normal angle ψ and the initial azimuth angle η are $89.8°$ and $180°$ respectively.   This case corresponds to Fig. 4b.   Initial wave number $k\rho$ is larger than the one for $f=f_q$, then it becomes smaller by outward propagation in the magnetosphere and return to $f \sim f_{UHR}$ with smaller $k\rho$ passing through the f_q resonance during propagation.

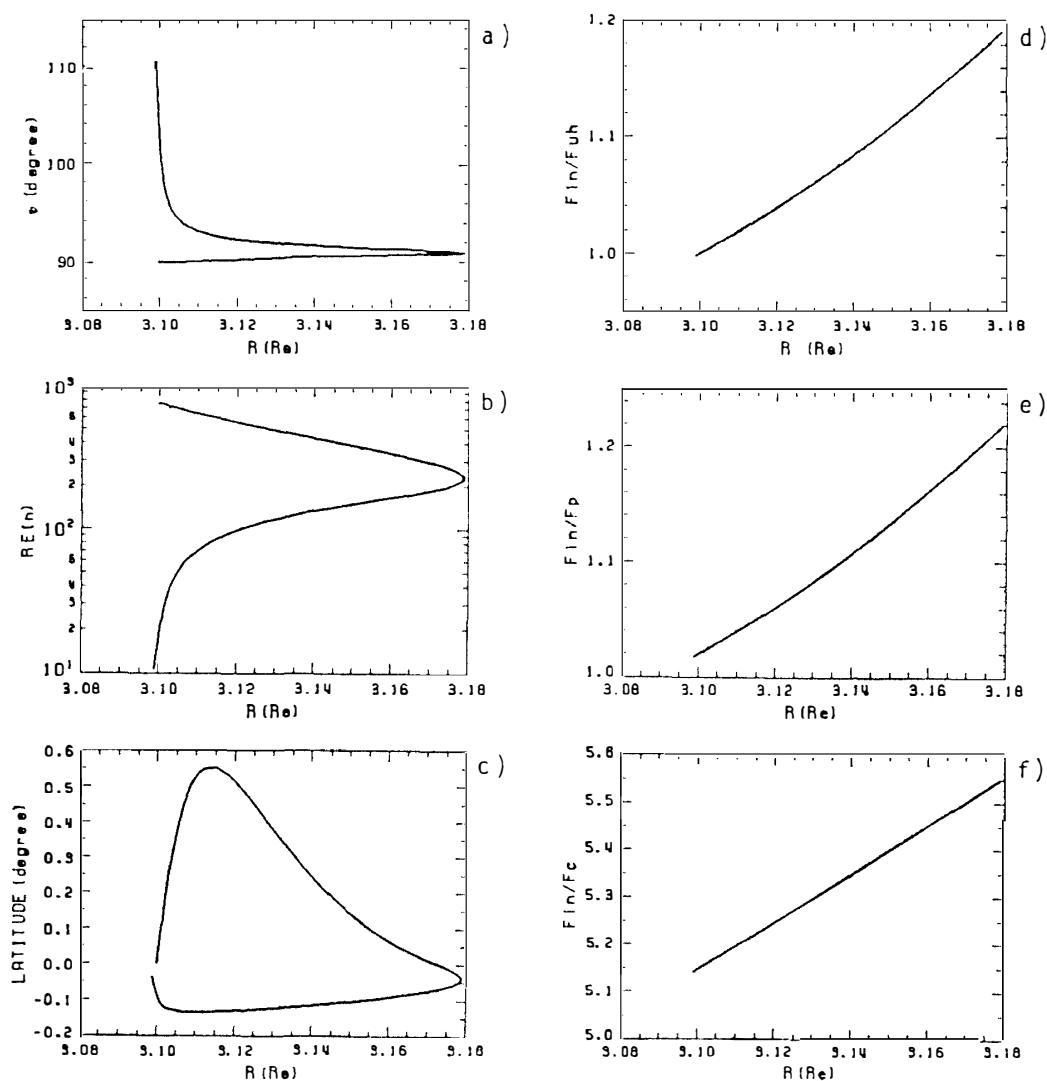In this case the ray path is directed to the north first, reflected back by refraction

Fig. 9.   Ray paths starting from 3.1 R_e under the plasmapause model (Fig. 3).

at a geomagnetic latitude of $0.55°$, and is directed to the south and outward. The path is then reflected by refraction at $R \simeq 3.18\ R_e$ and comes back to nearly the original point, where $f \cong f_{UHR}$. On the turning point at $R \simeq 3.18\ R_e$, the local f_q resonance frequency coincides with the wave frequency. The group velocity is directed almost perpendicular to k or parallel to B at f_{UHR} or f_q. In order for electrostatic waves to be converted to electromagnetic waves, electrostatic waves must arrive without damping at regions, where the wave normal angles are not close to $90°$. This feature implies that starting from the initial point located on the right side of the f_q peak (f_q resonance) in Fig. 4b the wave has, topologically, traversed to the left side of the f_q peak after passing through the f_q peak. The calculation of the ray path is terminated at a point where the electrostatic approximation is no longer valid. As shown in Fig. 9, the refractive index, initially as large as 10^8, continuously decreases along the path and finally becomes as small as 10. This fact suggests that the wave, which is originally electrostatic, can be converted to an electromagnetic (R-X-Z) mode wave.
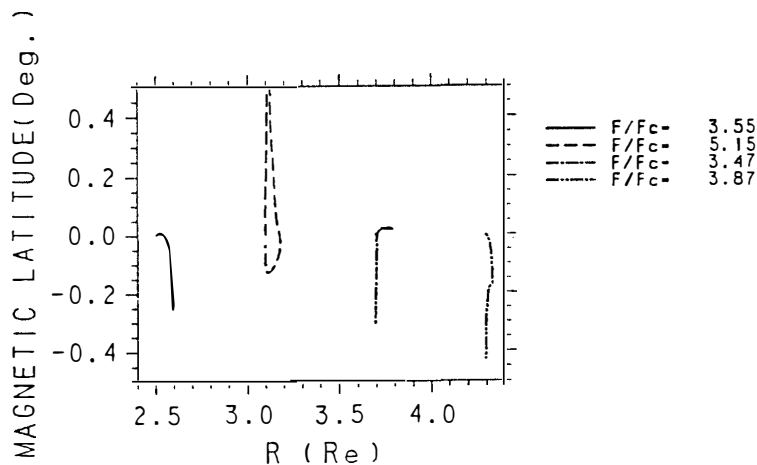

Fig. 10. Dependence of ray paths on starting distance under the plasmapause model (Fig. 3).

In Fig. 10, shown are ray paths starting from various distances on the geomagnetic equatorial plane initially with a condition that $f = f_{UHR}$ and with the same other initial conditions as in Fig. 9. The path shown in Fig. 9 is the broken line in Fig. 10. The path starting from $R = 2.5\ R_e$ is completely located inside the plasmasphere, whereas three other paths are outside the plasmapause. In either case, the paths starting from the right side of the f_q resonance, traverse, topologically, to the R-X-Z region after passing over the f_q resonance peak, and are terminated at the boundary between the electrostatic and electromagnetic regions.

On the other hand, at branches whose frequencies are less than f_q, the electrostatic dispersion does not much depend on the electron density (BARBOSA and KURTH, 1980). Therefore paths at these branches are not much affected by the plasmapause, and the results with the plasmapause are essentially same for an electron density profile without the plasmapause.

3.2.4. Electron temperature effect

So far, we have used the plasma temperature of 12000 K. However in the elec-

trostatic approximation the shape of the ray path is independent of the temperature, so that the ray path for a 1000 K plasma is the same as that for the 12000 K plasma. On the other hand, the propagation velocity is strongly dependent on temperature, or more precisely the velocity is proportional to the square root of temperature or the thermal speed. Therefore the time required for propagation is inversely proportional to $\sqrt{T}$. When the refractive index or $k\rho$ is not so large, and when therefore the electrostatic approximation becomes invalid or the waves become electromagnetic, their paths depend on temperature. The static waves become electromagnetic at a smaller $k\rho$ for a lower temperature.

3.3.   The results of ray tracing using the hot plasma dispersion relation

In the previous subsection, we have shown the results of ray tracing using the dispersion relation obtained by the electrostatic approximation. In the following, ray tracing under the hot plasma dispersion relation is compared with those under the
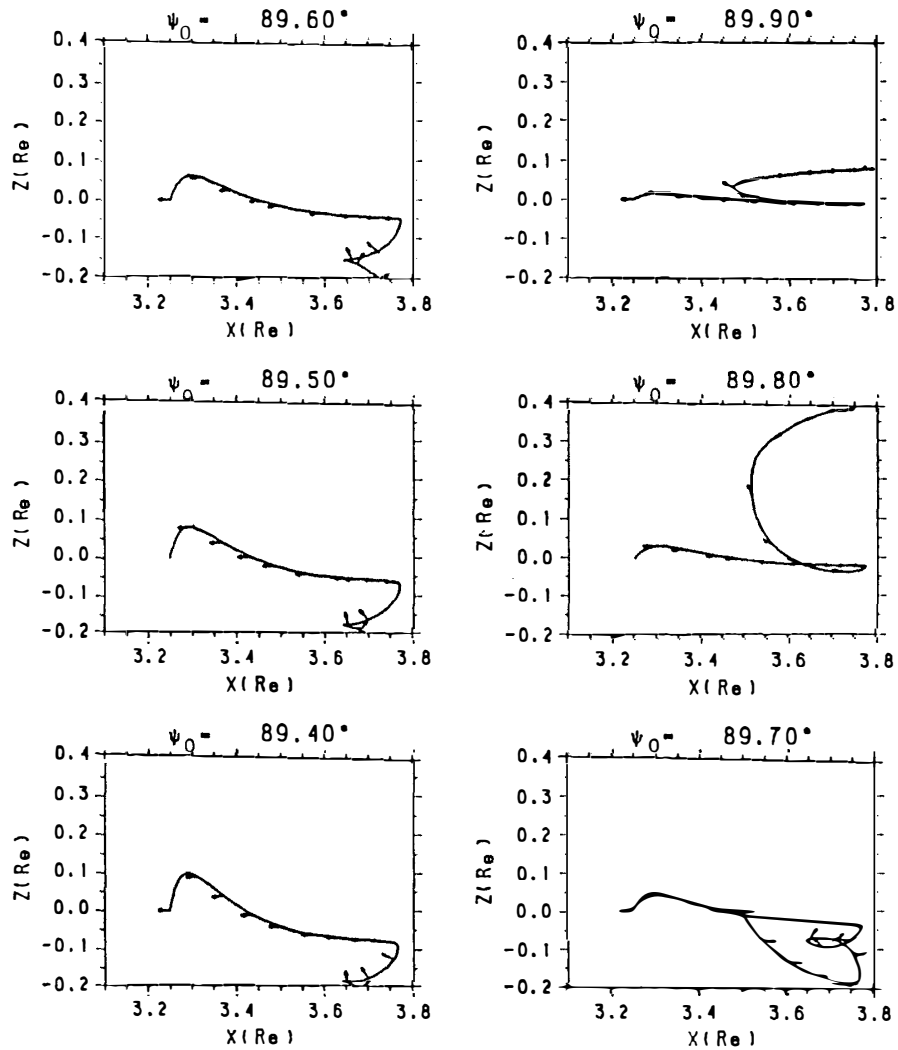

Fig. 11.   Ray paths in a hot plasma for a frequency of 28.015 kHz and for different initial wave normal angles $\psi = 89.4°-89.9°$.

electrostatic approximation, with similar initial conditions for ray tracing. In Fig. 11, the ray paths at 28.015 kHz(f/f_H=1.1), starting at 3.25 R_e and at the geomagnetic equator with the wave normal direction inward in the meridian plane, are shown for the initial wave normal angles ϕ_0=89.4–89.9°. Under the electrostatic approximation, the ray paths starting R=3.25 R_e with the same initial conditions as above are exactly identical with those shown in Fig. 6a until nearly the first turning points, around R=3.7–3.8 R_e, where the approximation conditions are violated.

It is, therefore, found that by the hot plasma ray tracing technique a ray path starting at a point where the electrostatic approximation is valid, can be continuously traced to a point where the approximation is not usable, that is, the wave becomes an electromagnetic mode wave.

Similarly, dependence of the ray paths on the initial wave normal angle in the range of ϕ_0=89.71–89.8° is shown in Fig. 12, with other parameters being kept the same as those in Fig. 11. From these figures, the ray paths actually show quite different features for slightly different initial wave normal angles after the reflection at a point where f is almost equal to the local f_P.

There are three cases when such a conversion occurs, dependent on the initial wave normal direction in the electrostatic mode, starting from the point A in Figs. 13a–13c.

In case Fig. 13a, from the point A the wave traverses through the point B to the point C, where the wave is reflected back by refraction to the same electrostatic mode. In the process B→C→B, the wave normal angle changed from 90° to 0° and again to nearly 90°. In case Fig. 13b, the initial wave from A passes through the point C where the mode converts from R-X-Z to L-X-Z, and reaches the point D where the wave is reflected back to C→B→A. In case Fig. 13c, the wave propagating from B to C reaches D where it is reflected back, but some energy can be converted to the L–O mode through the radio window at the point D.

Examples of parameter variations on these three cases are illustrated in Figs. 14–16, which correspond to the initial wave normal angle ϕ_0=89.6°, 89.8° and 89.74° respectively. The wave normal range for case (c) is 89.72° to 89.75°. The initial f/f_e is equal to 1.1 in these cases. If the wave starts at f/f_e=1.7 (3.775 R_e), that is, if it initially starts with a smaller $k\rho$ the range becomes wider, from 76° to 79°. In Fig. 14c, at point C which corresponds to the point C in Fig. 13a, the wave normal angle is zero and the group velocity vector is perpendicular to the direction of the geomagnetic field. On the other hand in Fig. 15c, similarly at point D, the wave normal angle ϕ is zero and the group velocity is parallel to the geomagnetic field. In Fig. 16c, at D, the situation is the same as in Fig. 15 and is quite similar to Fig. 4 of JONES (1980).

In the following, the process of mode conversion from R-X-Z to L-X-Z through the refractive index n=1 will be explained by using a refractive index surface diagram, in which real $n_{\parallel}$ and real $n_{\perp}$ are the components of the refractive index n, parallel and perpendicular to the external magnetic field. Namely, Fig. 17 illustrates refractive index surfaces at every 0.05 R from 3.5 to 3.75 R_e at the geomagnetic equator. In this figure, the broken line semi-circle at $|n|$=1 corresponds to the boundary between the R-X-Z mode and L-X-Z mode. Outside this circle represents the R-X-Z mode, whereas inside the circle represents the L-X-Z mode. A solid line, a dot-dash line and a broken
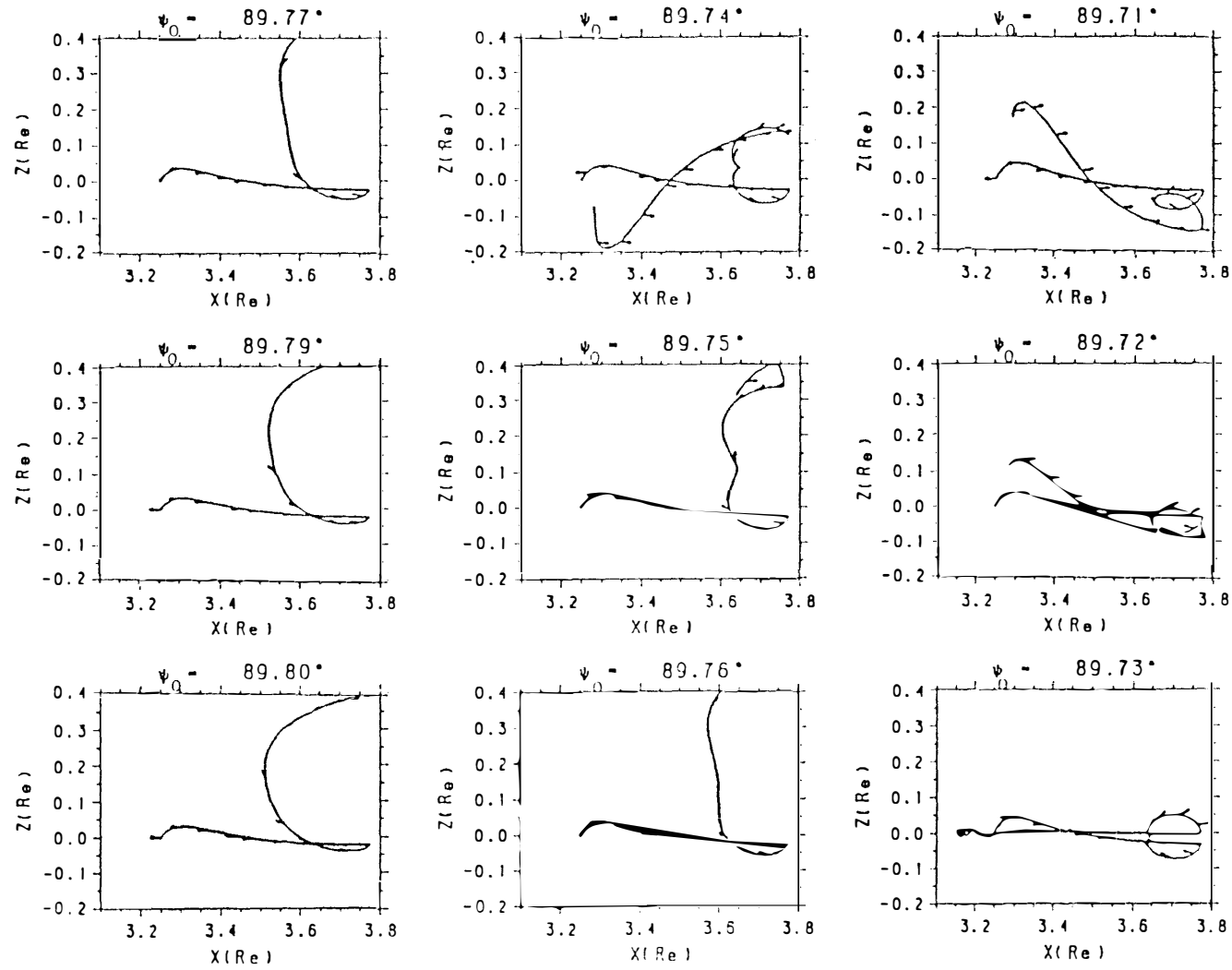
Fig. 12. Ray paths in a hot plasma for a frequency of 28.015 kHz and for a narrower range of the initial wave normal angles ψ=89.71°-89.8°.
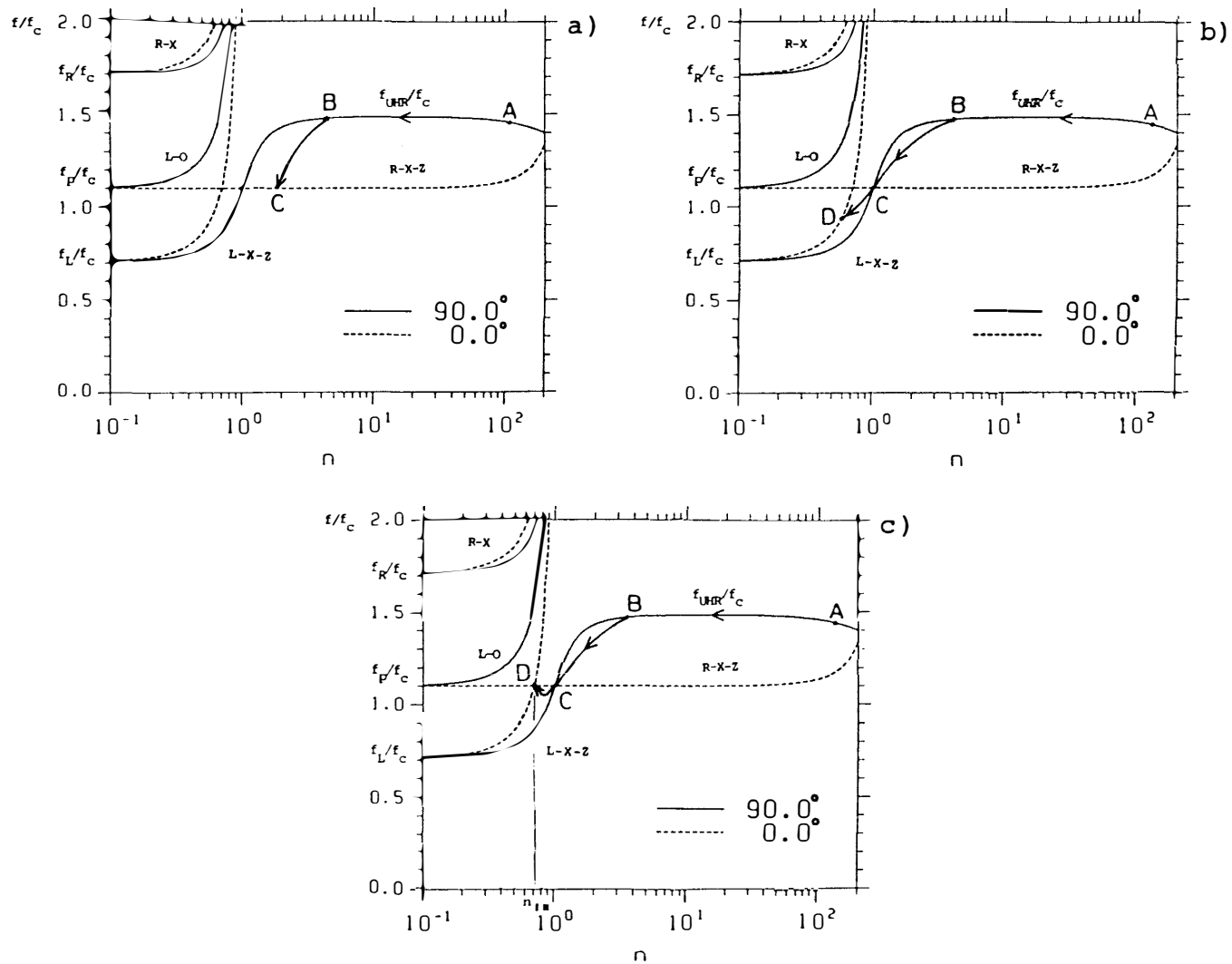
Fig. 13. Three different traverses of wave on the ω-k diagram depending upon the initial wave
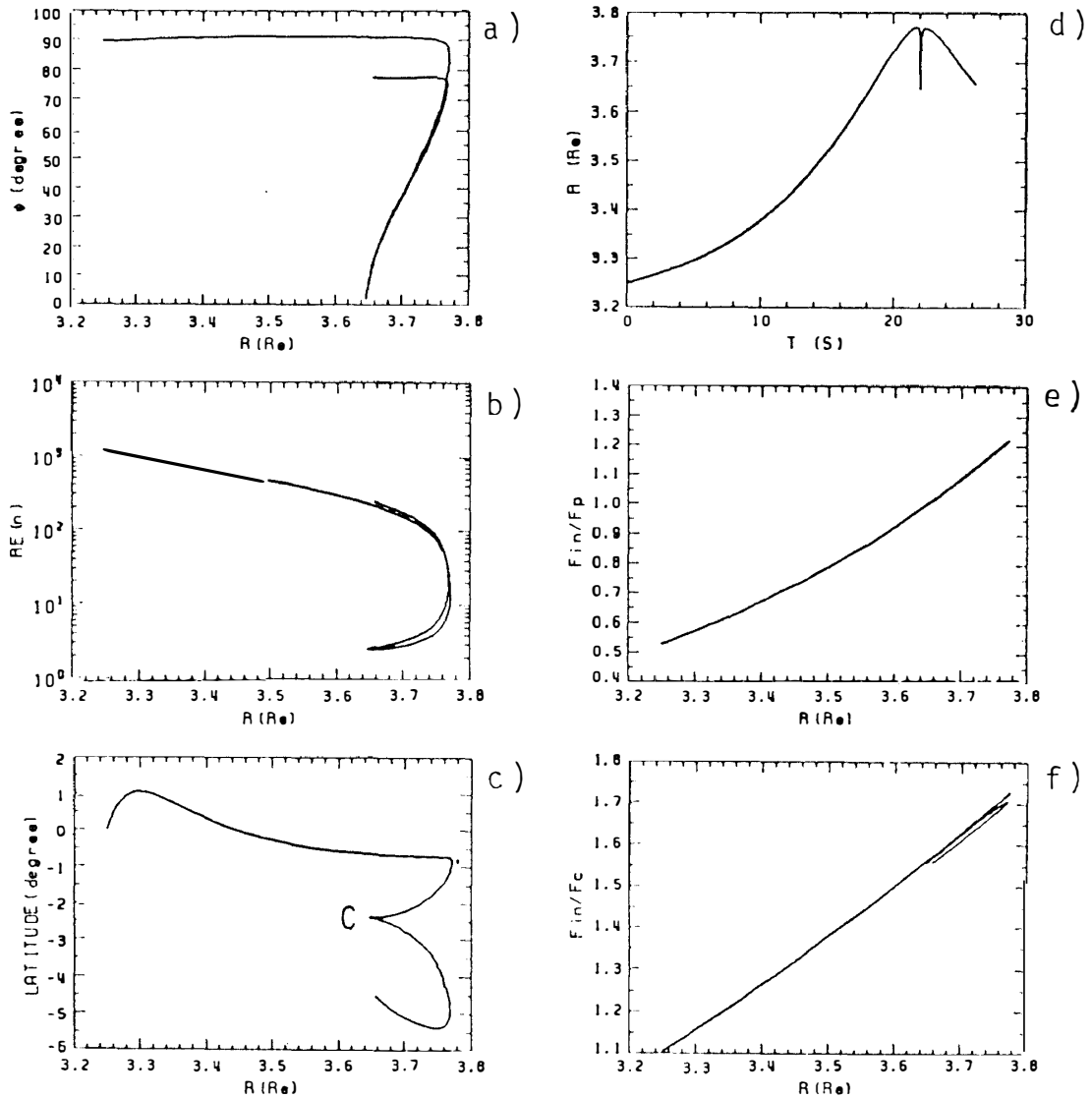normal direction.

Fig. 14.   Variation of parameters along the path corresponding to Fig. 13a.   The initial wave
normal angle is 89.6°.

line that cross the refractive index surfaces are the evolution of the refractive indices
for the paths of $\phi_0 = 89.6$, 89.76° and 89.8°, respectively.   Wave normal angles should
be in the second quadrant, although only the first and the fourth quadrants are shown
in Fig. 17 because the wave normal surfaces are symmetric about the *B* direction.
Arrows in the figure show the direction of the group velocity or the ray direction.
Figure 17b illustrates a more detail of Fig. 17a.

The solid line ($\phi_0 = 89.6°$) in Fig. 17a corresponds to the path from a point (*R*,
latitude) $\simeq$ (3.76 R_e, $-0.8°$) to (3.65 R_e, $-2.4°$) in Fig. 14c.   The ray direction is toward
the south initially and is directed to the earth, where wave normal is directed along the
B direction and the reflection occurs.   The wave normal angle quickly decreases for
decreasing *R* from 3.75 to 3.65 R_e.   The initial $n_{\parallel}$ in the *R-X-Z* mode is so large com-
pared with unity that the wave cannot be converted to the *L-X-Z* mode.   This case
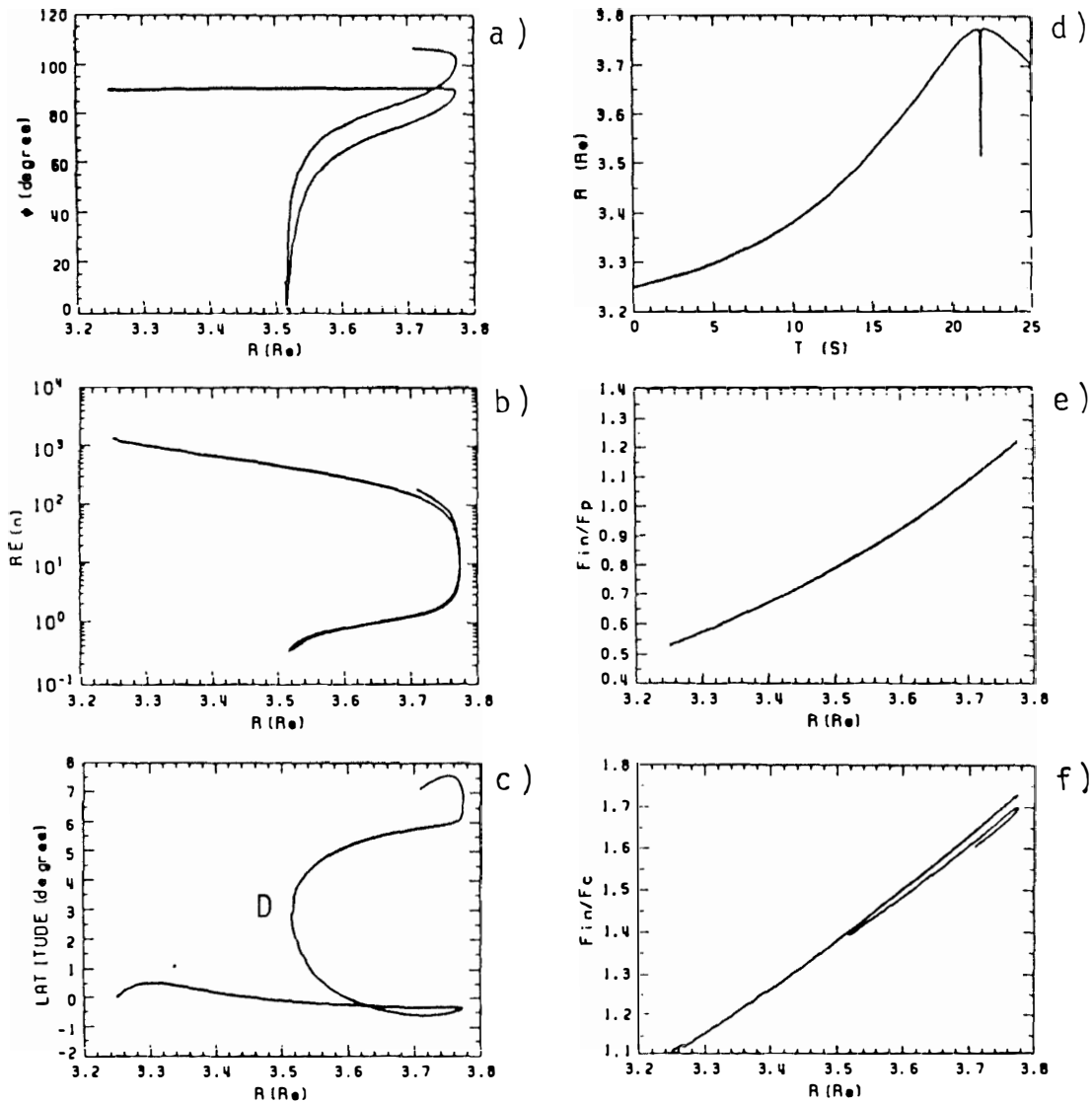corresponds to Fig. 13a.

Fig. 15. Variation of parameters along the path corresponding to Fig. 13b. The initial wave normal angle is 89.8°.

The dashed line $(\psi_0 = 89.8°)$ corresponds to the path from a point $(R, \text{latitude}) \simeq$ $(3.76\ R_e, -0.3°)$ to $(3.52\ R_e, 3°)$ in Fig. 15c. The arrows along the line in Figs. 17a and 17b show that the ray direction is toward the south initially and directed to the earth $(R=3.7)$ and to the north $(R=3.52)$, where both wave normal and group velocity are parallel to the geomagnetic field. The wave then continues to propagate with its wave normal direction in the first quadrant of the refractive index surface.

The dot-dash line $(\omega_0 = 89.74°)$ corresponds to the path from a point $(R, \text{latitude}) \simeq$ $(3.76\ R_e, -0.4°)$ to $(3.65\ R_e, 0.6°)$ in Fig. 16c. The arrows along the line in Figs. 17a and 17b show that the ray direction is toward the south initially and directed to the earth $(R=3.7\ R_e)$ and to the north $(R\simeq 3.63\ R_e)$. Until this point, the nature is similar to the above case, but the wave normal is not yet parallel to the geomagnetic field. Then the wave goes north and outward and the wave normal becomes parallel to B, where a part of the wave energy is converted to the L–O mode through the radio
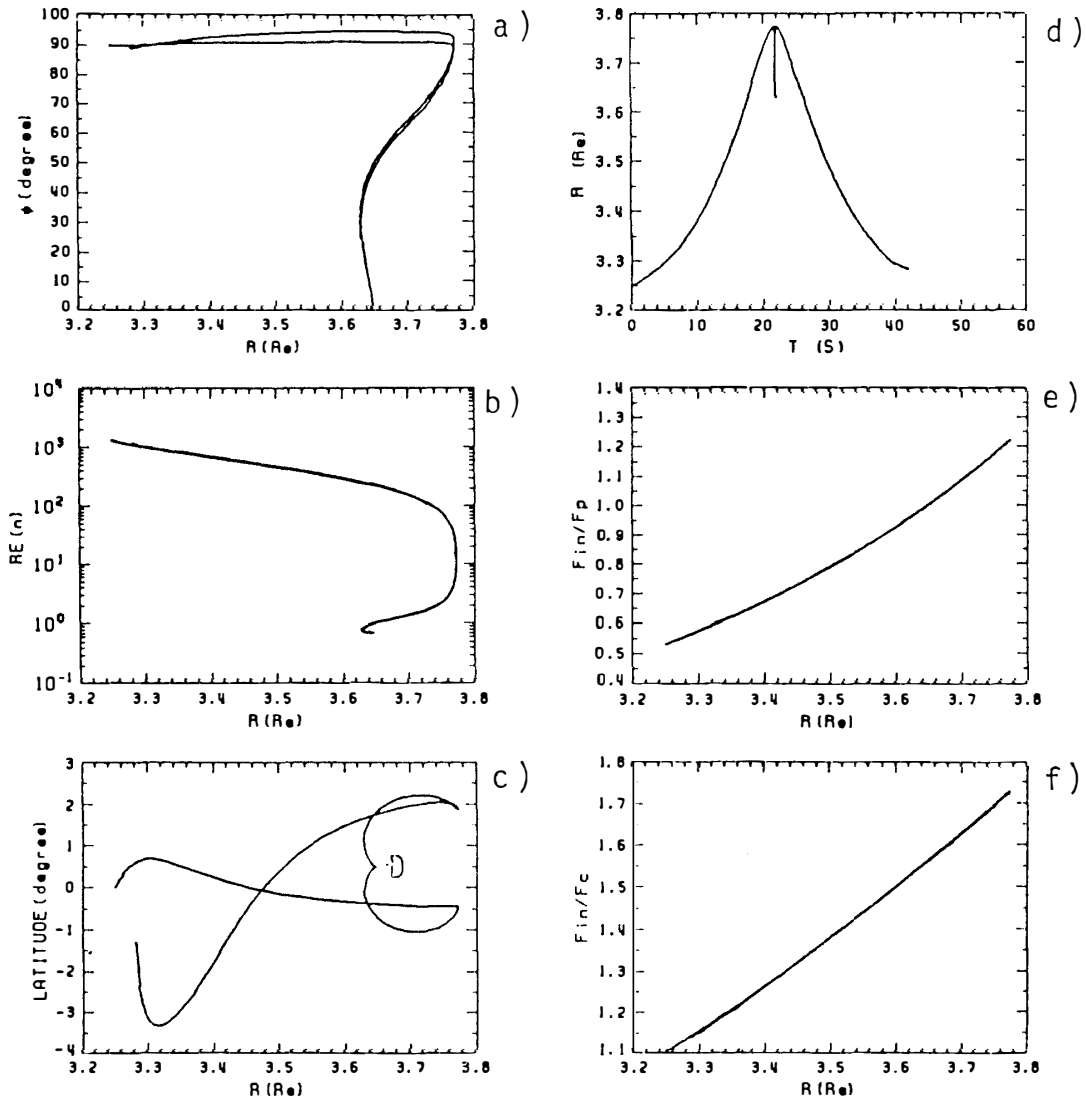
Fig. 16. Variation of parameters along the path corresponding to Fig. 13c. The initial wave normal angle is 89.74°.

window (BUDDEN, 1985). The rest of the wave energy is reflected there as the *L-X-Z* mode as shown in Fig. 16.

4. Discussion

We have shown that electrostatic waves starting at low latitudes (within a few degrees around the geomagnetic equator) are confined near the equatorial region and can propagate over several tenths of earth's radius without damping. Those starting at higher latitudes are damped soon. Although the initial wave normal angles are almost 90°, the component of *k* perpendicular to ∇B is conserved and is not so small except near the equator. Therefore, this component makes the wave normal angles smaller than 90° and then the waves are damped.
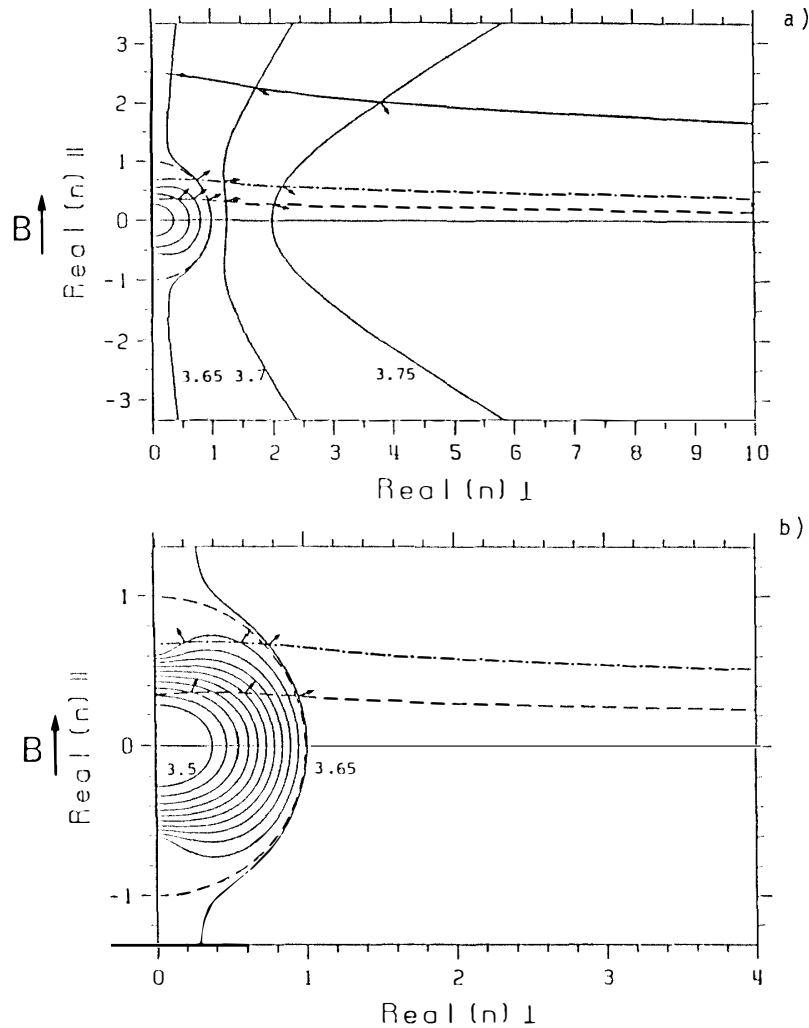
Fig. 17.   Variation of wave normal angles of the paths of Figs. 14–16 plotted on the refractive index surface.   The arrows show the ray directions.

The intense electrostatic waves are observed often in the equatorial region but the correlation with anisotropic electron flux is not so good. On the other hand, at higher latitudes electrostatic waves are observed much less often, but show good correlation with anisotropic electron flux (KURTH *et al.*, 1979). These facts are consistent with our results; namely at high latitudes large damping rate is expected, resulting in a small reception probability, and the emissions are only observed locally in the generation region, implying a good correlation with higher intensities of anisotropic electrons. Electrostatic waves starting at low latitudes in a meridian plane can propagate over long distances. And the wave number of these waves can become very small and the waves are converted to the Z-mode electromagnetic waves.

There are three cases when the conversion of the electrostatic cyclotron harmonic mode to the electromagnetic mode occurs as shown in Fig. 13. A mode conversion at the point D of case (c) is called the radio window (BUDDEN, 1985), where no sharp boundary is required. This mechanism is proposed by JONES (1980). Existence of

irregularities or sharp boundaries makes the conversion at the point D of case (b) possible. Better conversion rates are expected in these two cases (b) and (c). At the point C of case (a) a mode conversion to the L–O mode is also possible if there is a sharp plasma density change, as was suggested by OYA (1974). We have therefore confirmed again that these cases could explain a generation mechanism of continuum radiation. However, the initial wave normal angles of electrostatic electron cyclotron harmonic waves as the source must be in a small range close to 90°.

5. Conclusion

We have performed the 3-D ray tracing in a hot plasma with and without the electrostatic approximation in the magnetosphere. Under the electrostatic approximation, propagation characteristics of cyclotron harmonic waves are first examined. It is clarified that the waves starting near the equator can propagate over a long distance without damping and it is verified why the waves can be observed mostly near the equator. It is also clarified that in some cases wave number becomes very small and the waves could become electromagnetic. Ray tracing without the electrostatic approximation has confirmed mode conversion from cyclotron harmonic waves to Z-mode electromagnetic waves and clarified the conditions for the conversion. Further conversion to the L–O mode continuum radiation is possible but a strict constraint (narrow range of initial wave normal angle) is required. There are three cases when the conversion occurs and examples of paths corresponding to these cases are shown in Figs. 14 to 16 and are physically interpreted using the refractive index surfaces. In an electron density model with the plasmapause, ray paths which can go over the f_q resonance are successfully shown and physically explained.

We believe that this program is valuable and could help further understanding of a lot of phenomena in the magnetosphere.

Acknowledgments

References

AIKYO, K. and ONDOH, T. (1971): Propagation of nonducted VLF waves in the vicinity of the plasmapause. J. Radio Res. Lab., 18, 153–181.

BARBOSA, D. D. and KURTH, W. S. (1980): Superthermal electrons and Bernstein waves in Jupiter's inner magnetosphere. J. Geophys. Res., 85, 6729–6742.

BUDDEN, K. G. (1985): The Propagation of Radio Waves; The Theory of Radio Waves of Low Power in the Ionosphere and Magnetosphere. Cambridge, Cambridge Univ. Press, 669 p.

HASHIMOTO, K. (1985): Propagation modes of auroral kilometric radiation; A review. Mem. Natl Inst. Polar Res., Spec. Issue, 36, 149–158.

JONES, D. (1980): Latitudinal beaming of planetary radio emissions. Nature, 288, 225–229.

JONES, D. (1981): First remote sensing of the plasmapause by terrestrial myriametric radiation. Nature, 294, 728–730.

KIMURA, I. (1985): Whistler mode propagation in the earth and planetary magnetospheres and ray

tracing techniques.   Space Sci. Rev., **42**, 449–466.

KURTH, W. S., CRAVEN, J. D., FRANK, L. A. and GURNETT, D. A. (1979):   Intense electromagnetic waves near the upper hybrid resonance frequency.   J. Geophys. Res., **84**, 4145–4164.

LEMBEGE, B. and JONES, D. (1982): Propagation of electrostatic upper-hybrid emission and Z mode waves at the geomagnetic equatorial plasmapause.   J. Geophys. Res., **87**, 6187–6201.

MIYAMOTO, K. (1976): Kakuyûgô no tameno Purazuma Butsuri (Plasma Physics for Nuclear Fusion). Tokyo, Iwanami, 559 p.

OHNUMA, T., WATANABE, T. and SANUKI, H. (1982):   Spatial investigation of mode conversion between an electrostatic cyclotron harmonic wave and an electromagnetic ordinary wave. Radio Sci., **17**, 1633–1636.

OYA, H. (1974):   Origin of Jovian decametric wave emissions -Conversion from the electron cyclotron plasma wave to the ordinary mode electromagnetic wave.   Planet. Space Sci., **22**, 687–708.

WEINBERG, S. (1962):   Eikonal method in magnetohydrodynamics.   Phys. Rev., **126**, 1899–1909.